Pinto et al., http://www.jcb.org/cgi/content/full/jcb.201509039/DC1

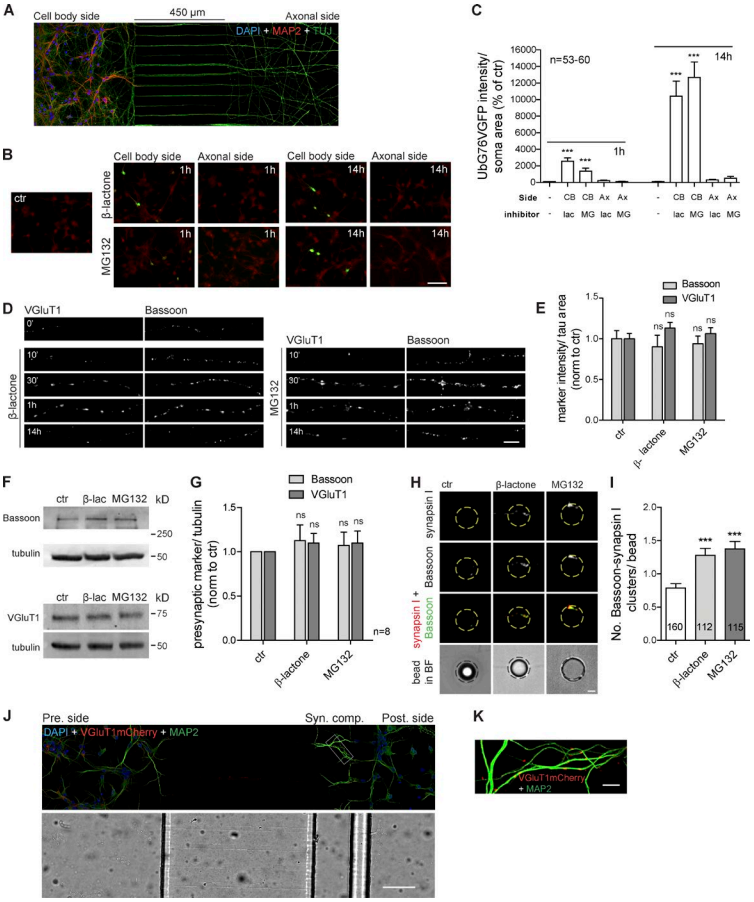

Figure S1. **Enhanced presynaptic clustering after specific inhibition of the proteasome in axons.** (A) Dissociated rat embryonic hippocampal neurons were plated in the cell body side of a microfluidic platform (Taylor et al., 2005), allowed to grow until DIV 7, and then immunostained for MAP2 (red) and Tuj1 (green). Axons extended through the set of 450-µm microgrooves, and a pure population of axons was obtained on the axonal side. (B) Specific proteasome inhibition in isolated axons in microfluidic devices. To validate inhibition of the proteasome specifically in axons, thus confirming that locally applied proteasome inhibitors do not affect proteasome activity at the cell body level, the degradation reporter $Ub^{G76V}GFP$ (Dantuma et al., 2000) was expressed, and its intensity in somas (MAP2 staining, red) was analyzed after inhibition of the proteasome for 1 or 14 h on either side of the compartment. To accomplish this, 1 µM MG132 and 10 µM β-lactone, two mechanistically distinct proteasome inhibitors, were used. This treatment did not affect neuron viability or induce axon degeneration (unpublished data). $Ub^{G76V}GFP$ is a GFP-based reporter substrate for proteasome degradation; it consists of an uncleavable N-terminal Ub mutant (Ub^{G76V}) in frame with GFP. The Ub moiety is recognized as a degradation signal, thus potentiating its further polyubiquitination and degradation by the proteasome (Dantuma et al., 2000). Accordingly, the reporter is constitutively degraded within the cell and will accumulate if UPS degradation halts, resulting in an increased signal intensity, or vice versa. As expected, when expressed in the cell body side of microfluidic devices, $Ub^{G76V}GFP$ only suffered changes to its intensity when proteasome inhibitors were added to the soma side. Therefore, microfluidic devices allow for the specific inhibition of the proteasome in axons and so are useful tools for the study of proteasome involvement in axon-intrinsic mechanisms. Bar, 50 µm. (C) Change in reporter intensity in somas per MAP2 area (percentage of control). Increased reporter intensity was observed when proteasome inhibitors (lac, β-lactone; MG, MG132) were added to the cell body side (CB) but not when added to the axonal side (Ax). *n*, microscope FOVs. Three independent experiments. (D) Individual images for VGluT1 and Bassoon staining (correspondent to Fig. 1 B). Bar, 5 µm. (E) Quantitative values of total Bassoon and VGluT1 intensity per tau area in immunostained isolated axons after treatment for 1 h with proteasome inhibitors or vehicle. Quantification was performed in the same images used for quantification of presynaptic clusters in Fig. 1 C. A total of 36 FOVs were analyzed per condition in three independent experiments. (F) Analysis of presynaptic markers' expression levels upon proteasome inhibition. Total cell lysates were obtained from DIV 7 hippocampal neurons after treatment with proteasome inhibitors or vehicle for 1 h, and WB for VGluT1 and Bassoon was performed. Tubulin, loading control. Proteasome inhibitors did not alter total levels of presynaptic markers, thus discarding the possibility that proteasome inhibition-induced clustering would be an artifact of a random increased amount of the protein. (G) Quantitative levels of presynaptic markers relative to the loading control (normalized to control). *n*, individual experiments. (H) Formation of presynaptic clusters on beads (dashed circles) after proteasome inhibition. Beads were added to the axonal compartment for 3 h, and then axons were treated with proteasome inhibitors or vehicle for 1 h and immunostained for Bassoon (green) and synapsin I (red). Axonal proteasome inhibition further enhanced formation of presynaptic clusters on beads. Bar, 5 µm. BF, brightfield. (I) Quantitative data of the number of Bassoon puncta colocalizing with synapsin I puncta per bead. *n*, beads. Two independent experiments. (J) In synapse formation chambers, three compartments are separated by two sets of microgrooves of different lengths (Taylor et al., 2010). The presynaptic compartment and the postsynaptic compartment are connected to the middle synaptic compartment by 450-µm and 75-µm microgrooves, respectively. Because of the short length of the second set of microgrooves, dendrites coming from the postsynaptic compartment reach the synaptic compartment, in which they will have contact with axons derived from the presynaptic compartment. Expression of the presynaptic marker VGluT1mCherry by a lentiviral system on the presynaptic compartment (Pre. side) results in several growing axons extending into the synaptic compartment (Syn. comp.). Poststaining for MAP2 (green) and DAPI (blue) was performed to locate somatodendritic structures. The signal for MAP2 was differently adjusted in the synaptic compartment to minimize differences in signal intensity. Several dendrites crossed the short set of microgrooves, reaching the synaptic compartment. Bottom, correspondent brightfield image. Bar, 100 µm. (K) Enlarged image of box in J. VGluT1mCherry puncta formed along dendrites on the synaptic compartment. Bar, 10 µm. ***, $P < 0.001$ compared with control (Kruskal-Wallis test followed by the Dunn's multiple comparison test). ns, not significant. Results are presented as mean values ± SEM.

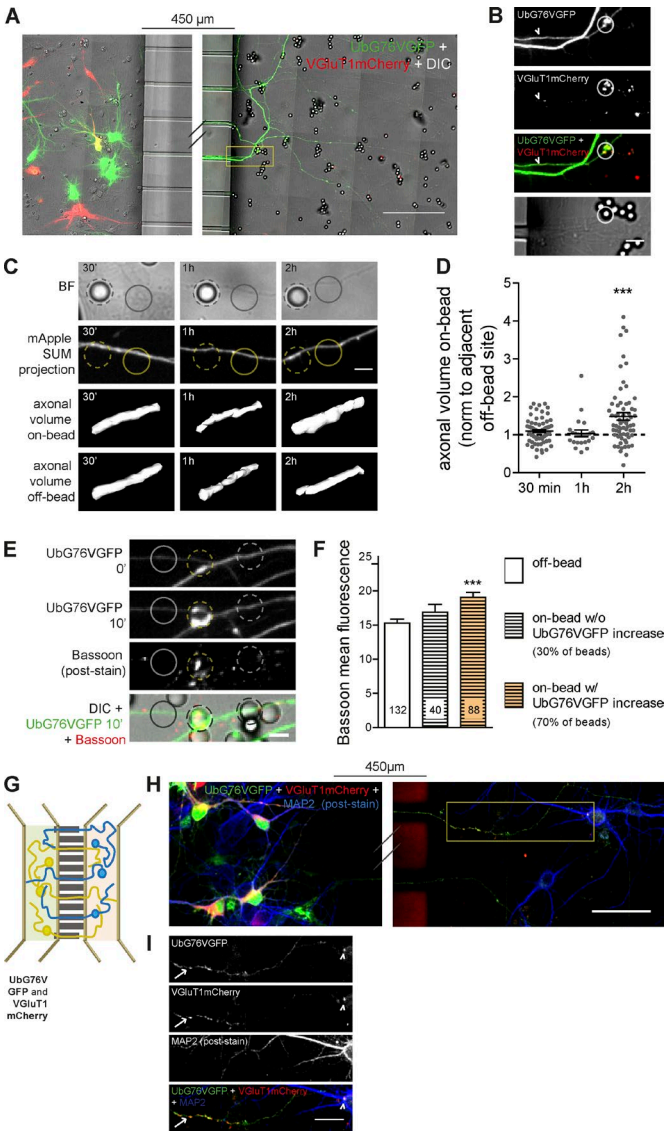

Figure S2. **Rapid increase in the intensity of a degradation reporter precedes and accompanies clustering of presynaptic material.** (A) Experimental setup to monitor axonal changes upon bead contact. Dual Sindbis viral expression for the presynaptic reporter VGluT1mCherry (red) and the degradation reporter Ub^{G76V}GFP (green) on the somal side of microfluidic devices. Infected axons reached the axonal compartment, and subsequently, beads were added, and their effect on the contacting axon was monitored by time-lapse imaging every 10 min (Fig. 2 A). The signal for Ub^{G76V}GFP and VGluT1mCherry was differently adjusted between right and left image to prevent oversaturation of signal at the soma level. Bar, 100 µm. (B) Enlarged image of box in A showing a dually infected axon (GFP$^+$ and mCherry$^+$, arrowheads) extending into the axonal compartment and establishing a contact with a bead (white circles). Bar, 10 µm. (C) Axonal volume at on-bead and off-bead sites. Neurons in microfluidic devices were infected with Sindbis virus expressing mApple for total filling, and beads were added to the axonal side for the indicated periods of time. Z stacks were acquired, and axonal volume at on-bead (dashed circle; images in third row) and off-bead (solid circle; images in fourth row) was obtained by 3D surface reconstruction in ImageJ with the plug-in ImageJ 3D viewer. SUM, summation of all slices of the z stack. BF, brightfield. No changes in axonal volume were observed up to 1 h of bead contact. (D) Quantification of axonal volume on beads. In the brightfield image, ROIs for beads and adjacent off-bead sites were created and used in the corresponding mApple z stack for quantification of axonal volume by the ImageJ plug-in 3D object counter. Results are normalized to the corresponding off-bead site (dashed line). A total of 73 (30 min), 43 (1 h), and 68 (2 h) beads were analyzed from two independent experiments. (E) Posthoc clustering of active zone material on beads that reduced axonal proteasome activity. After time-lapse (4–5 h after addition of beads), cultures were fixed and stained for Bassoon (red). Clustering of Bassoon was more pronounced on beads at which increased intensity of Ub^{G76V}GFP at 10 min was detected (yellow vs. white dashed circles). Solid circles indicate off-bead sites. (F) Bassoon raw intensity values in off- and on-bead sites. Beads were divided according to their capacity to increase Ub^{G76V}GFP intensity in the contacting axon above off-bead levels at 10 min (~70% and 30% of beads with and without increases in Ub^{G76V}GFP intensity, respectively). *n*, beads and equivalent off-sites. Three independent experiments. (G) Experimental setup to monitor changes in the axonal domain undergoing presynaptic differentiation onto dendrites. Neurons were plated on either sides of microfluidic devices and dually infected with Sindbis virus expressing Ub^{G76V}GFP and VGluT1mCherry on only one side. Coinfected axons (yellow) reached the opposite compartment, in which they established synaptic contacts with resident noninfected neurons (blue). Dually infected axons were imaged every 10 min for at least 5 h in the microfluidic devices' compartments opposite to viral infection (Fig. 3, A–D). Imaging was performed on the compartment opposite to infection in a way of guaranteeing that the quantified signal is axon specific, without contribution from the postsynaptic cell. (H) Postimaging. Retrospective labeling for MAP2 (blue) was performed to detect dendrites. The signal for Ub^{G76V}GFP (green) and VGluT1mCherry (red) was differently adjusted between right and left image to prevent oversaturation of signal at the soma level. Bar, 50 µm. (I) Enlarged image of box in H showing a coinfected axon (GFP$^+$ and mCherry$^+$; arrows) extending into the opposite compartment and forming a presynaptic cluster (arrowheads) on a MAP2$^+$ cell body. Bar, 20 µm. ***, $P < 0.001$ compared with off-bead (Kruskal-Wallis test followed by the Dunn's multiple comparison test). (C and E) Bars, 5 µm. Results are presented as mean values ± SEM.

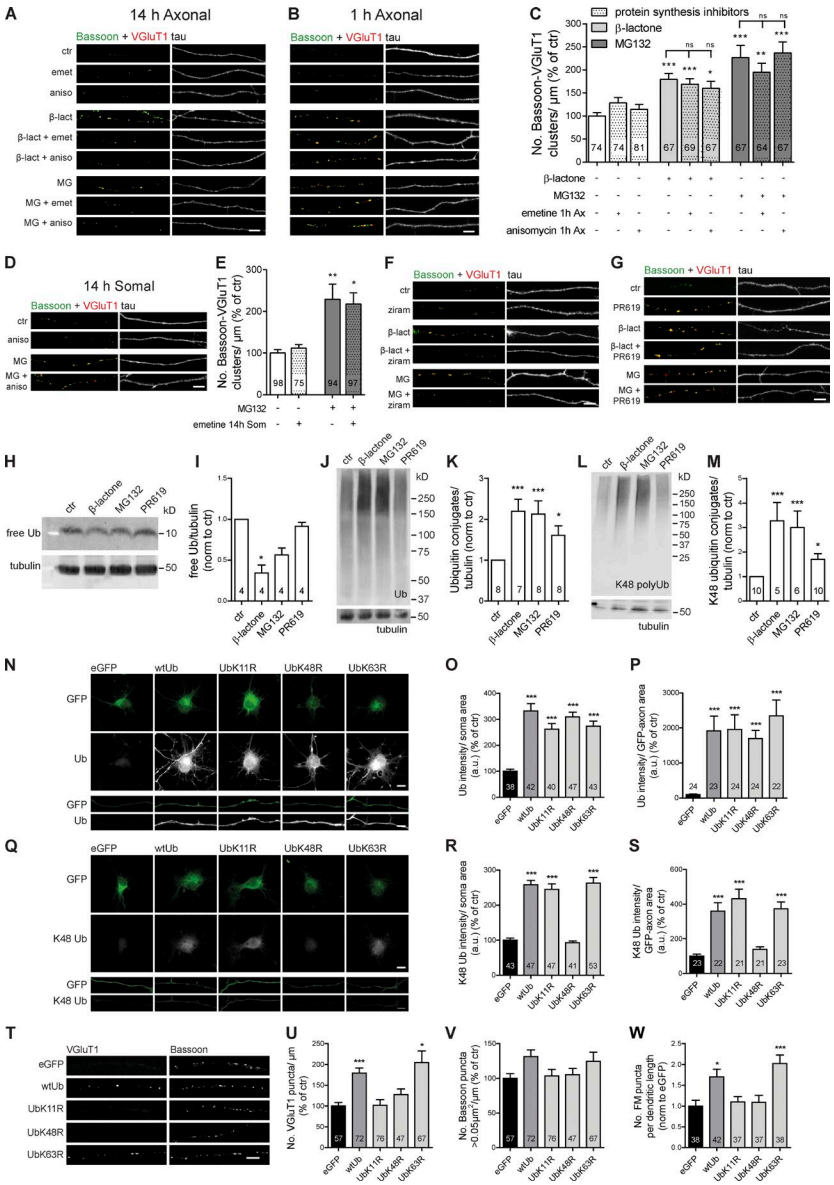

Figure S3. **Presynaptic assembly and levels of conjugated Ub upon protein synthesis and UPS inhibitors and overexpression of Ub and its mutant forms.** (A, B, D, F, and G) Representative images of presynaptic clusters (Bassoon [green] + VGluT1 [red]) and tau (white) for the effect of long-term axonal (14 h; A), acute axonal (1 h; B), and long-term somal (14 h; D) protein synthesis inhibitors (with emetine or anisomycin), the E1 inhibitor ziram (F), and the deubiquitinases inhibitor PR619 (G). Correspondent quantitative data are shown in Fig. 4 B, this figure (C and E), and Fig. 4 (C and D) for A, B, D, F, and G, respectively. emet, emetine; aniso, anisomycin; β-lact, β-lactone; MG, MG132. Bars, 5 µm. (C and E) Number of presynaptic clusters per axonal length for acute axonal (1 h; Ax; C) and long-term somal (14 h; Som; E) protein synthesis inhibition (percentage of control). *n*, microscope FOVs. Four to five independent experiments. ns, not significant. (H, J, and L) Effect of proteasome inhibitors and PR619 on the levels of free and conjugated Ub. Total cell lysates were obtained from DIV 7 neurons after 1-h treatment with β-lactone, MG132, PR619, or vehicle. Analysis by WB for Ub to examine levels of free Ub (H) and ubiquitinated conjugates (J) and for K48 polyUb (L) was performed. Tubulin, loading control. As expected, proteasome inhibitors strongly up-regulated the levels of ubiquitinated conjugates (J) while reducing free Ub levels (H). (J) The deubiquitinase inhibitor PR619 also elevated levels of ubiquitinated conjugates, although with a lower effectiveness. (L) Increases in the levels of K48 polyubiquitinated proteins are also visible for both proteasome inhibitors and PR619. (I, K, and M) Quantification of band intensities relative to control conditions. *n*, individual experiments. (N and Q) Validation of constructs for wtUb and its lysine-specific mutant forms. Neurons were infected with Sindbis virus expressing wtUb, Ub mutants that prevent formation of specific types of polyUb chains (UbK11R, UbK48R, and UbK63R), and eGFP as control. Levels of endogenous Ub (N; white) and K48 polyUb (Q; Apu2 antibody, white) were evaluated on GFP+ neurons by immunocytochemistry both at the cell body and axon level. Neurons were plated as pseudo-explants so that the majority of axons are isolated. (N) Regardless of the mutation, overexpression of wtUb and its mutant forms up-regulated levels of Ub in comparison to eGFP. (Q) Expression of Ub constructs also induced accumulation of K48-conjugated Ub in cells, which was abrogated when the specific lysine was mutated. This validation was performed by staining for K48 polyUb. Nevertheless, we assume that the same holds true for the other type of chains and respective mutants. Bars: (top) 10 µm; (bottom) 5 µm. (O, P, R, and S) Quantification of Ub (O and P) and K48 polyUb (R and S) intensity per soma area (O and R) and axon area (P and S; percentage of control). *n*, (O and R) cells; (P and S) microscope FOVs. Two independent experiments. a.u., arbitrary units. (T) Representative VGluT1 and Bassoon images after expression of wtUb and its mutants (see Fig. 5, B and C, for merge and tau images and quantitative data, respectively). Bar, 5 µm. (U–W) Additional presynaptic parameters quantified after expression of wtUb and Ub mutants. Quantitative values of number of VGluT1 puncta per axonal length (U), number of Bassoon puncta bigger than 0.05 µm^2 per axonal length (V), and number of total FM puncta on dendrites (W). *n*, (U and V) microscope FOVs; (W) dendrites. ***, $P < 0.001$; **, $P < 0.01$; and *, $P < 0.05$ compared with control (Kruskal-Wallis test followed by the Dunn's multiple comparison test). Columns without asterisks do not reach significance. Results are presented as mean values ± SEM.

References

Dantuma, N.P., K. Lindsten, R. Glas, M. Jellne, and M.G. Masucci. 2000. Short-lived green fluorescent proteins for quantifying ubiquitin/proteasome-dependent proteolysis in living cells. *Nat. Biotechnol.* 18:538–543. http://dx.doi.org/10.1038/75406

Taylor, A.M., M. Blurton-Jones, S.W. Rhee, D.H. Cribbs, C.W. Cotman, and N.L. Jeon. 2005. A microfluidic culture platform for CNS axonal injury, regeneration and transport. *Nat. Methods.* 2:599–605. http://dx.doi.org/10.1038/nmeth777

Taylor, A.M., D.C. Dieterich, H.T. Ito, S.A. Kim, and E.M. Schuman. 2010. Microfluidic local perfusion chambers for the visualization and manipulation of synapses. *Neuron.* 66:57–68. http://dx.doi.org/10.1016/j.neuron.2010.03.022